1 Supporting Information

2 Chlorine/UV Treatment of Anatoxin-a by

3 Activation of the Amine Functional Group

4 **Moshan Chen[1] and Ernest R. Blatchley III[1,2,*]**

5 [1]Lyles School of Civil Engineering, Purdue University, West Lafayette, IN, 47907, USA

6 [2]Division of Environmental & Ecological Engineering, Purdue University, West Lafayette,

7 IN, 47907, USA*Corresponding Author: Phone: 1-765-494-0316; email: blatch@purdue.edu

9

10 **Section S1.** Preparation of [Cl-DMA] Stock solution

11 The stock solution of ANTX-a (fumarate) was prepared by adding 1.4-1.5 mL water

12 from a Barnstead[TM] nanopure (18.2 mΩ) system directly into the vial from Cayman

13 Chemical, contained in a 25-mL beaker on an analytical balance. Prior to use, the vial was

14 stored in the dark at -20°C. Working solutions were freshly prepared daily from the stock

15 solution and stored at 4°C.

16 Stock solutions of dimethylamine (DMA) were prepared by 100X dilution of a

17 commercially available DMA aqueous solution (Acros, 40% wt%, ρ=0.890 g/mL), stored in a

18 sealed and dark condition, and used for a maximum of 7 days. N-chlorodimethylamine (Cl-

19 DMA) stock solutions were directly prepared by mixing free chlorine into a solution with a

20 known (gravimetrically determined) concentration of DMA with a Cl:N molar ratio of 0.5

21 (Cl:N=1:2). A DPD colorimetric test verified that under this condition, 99% of free chlorine

22 was consumed. pH was adjusted with 0.5 M NaOH and 0.5 M HCl.

23 Inorganic salts including dibasic potassium phosphate (Macron Chemicals, $\geq$ 99%) and

24 monobasic potassium phosphate (Macron chemicals, $\geq$ 99%), were analytical grade.

25

26 **Section S2.** Operation of a Capillary UV System with Uridine as a Chemical Actinometer
27   The capillary UV reactor reduces the potential for loss of volatile compounds, as
28 compared to the collimated beam UV reactor, and could be connected directly to the
29 membrane-introduction mass spectrometry (MIMS) system to accomplish analysis and avoid
30 loss in transfer of solution. A schematic illustration of the capillary reactor is presented in
31 Figure S1.
32
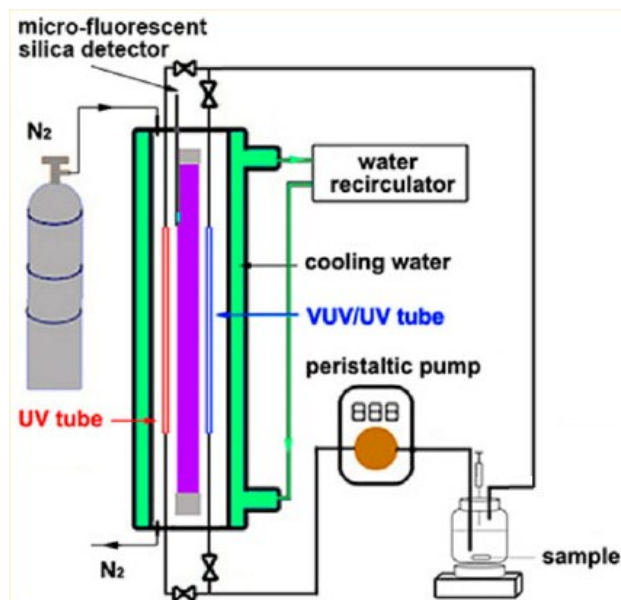
33

34   **Figure S1.** Schematic illustration of capillary UV reactor of Li et al. [1]. For experiments
35   described herein, only the "UV tube" was used, which allowed exposure to radiation at a
36   characteristic wavelength of 254 nm.

37   Chemical actinometry was used to measure the UV_{254} dose (D) received by the
38 solution when flowing through the capillary UV reactor.[2,3] Jin et al. applied an aqueous
39 solution of uridine (URD, $C_9H_{12}N_2O_6$), with a known quantum yield and a known molar
40 absorption coefficient at 254 nm [2]. Fig. S2 below illustrates the procedure described by Jin et
41 al. and used in the present experiment [2]. Eq (S1) indicates that the UV_{254} dose applied to the
42 actinometer could be indirectly calculated through the decrease in concentration of the URD
43 actinometer [2].
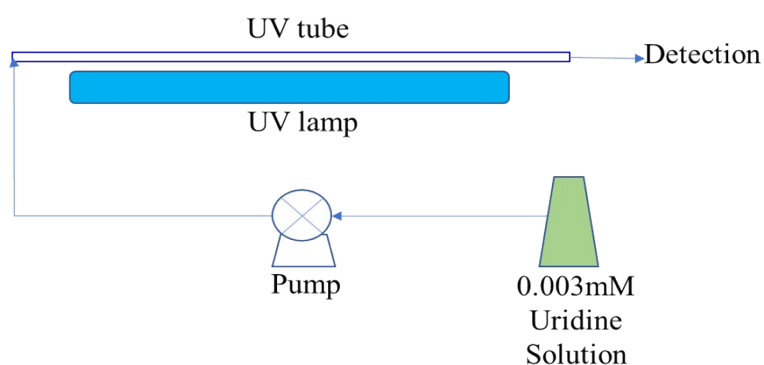
44
45   **Figure S2.** Chemical Actinometry Schematic Diagram.

46

$$D = \frac{ln^{\boxed{io}}(A_{262nm}^{0}/A_{262nm})}{2.303 \times 1000 \times \epsilon_\lambda \times \Phi \times t} \times Q \times t \qquad (S1)$$

where D is the measured UV_{254} dose, A_{262nm} is the absorbance measured for URD at 262 nm, which corresponds to its peak and is used as a surrogate measurement for its concentration. ϵ_λ is the molar absorption coefficient of uridine at the wavelength of λ. To be consistent with the low-pressure UV lamp used in this and the subsequent photochemical experiments, λ was chosen to be 254 nm. Φ is the quantum yield of URD, which is reported by Jin et al. as 0.020 mol E^{-1}, the mean value calculated from three published studies [2]. Q is the total photon energy of one einstein of photons at a given wavelength. $Q = N_A * h\nu$, where N_A is Avogadro's constant, h is the Planck constant, and ν is the frequency of the applied radiation.
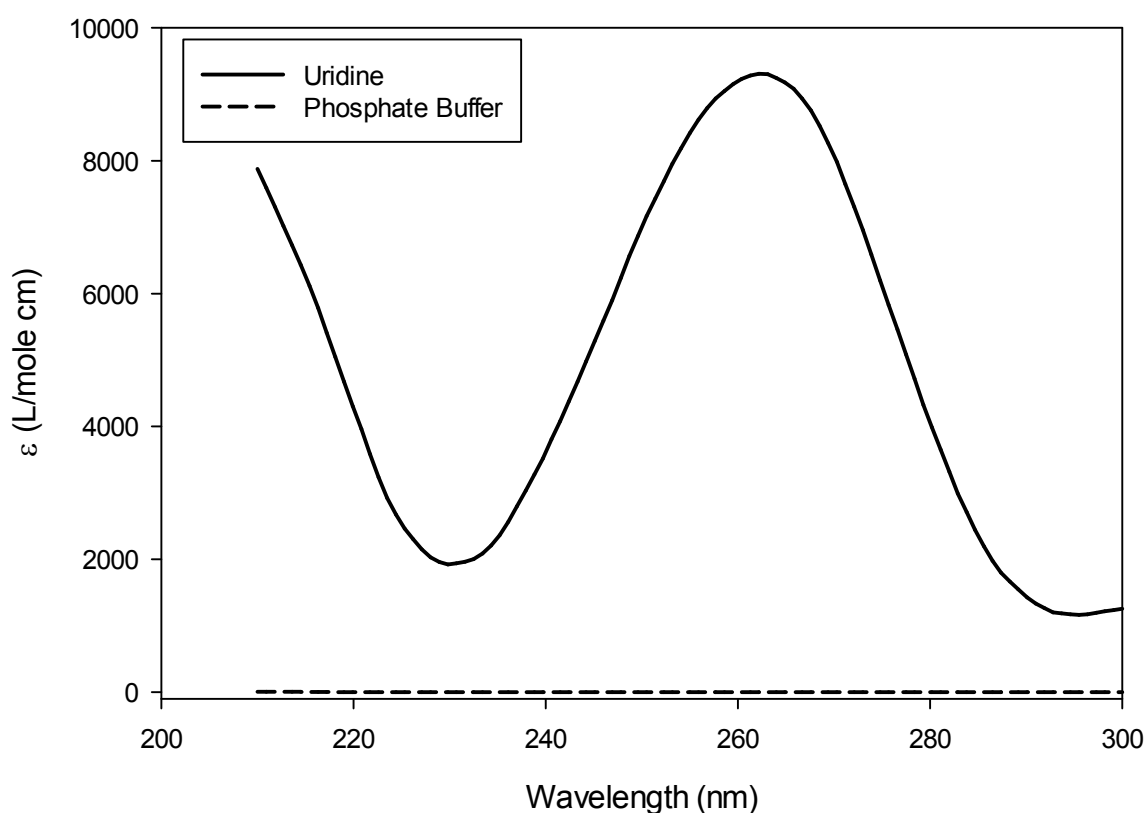
Figure S3. Molar absorption spectrum of uridine (pH=7.0 with 10 mM phosphate buffer, [URD]=3 μM).   Also included is the absorption spectrum of the phosphate buffer.

Fig. S3 illustrates the UV absorption spectrum of URD (standard solution: [URD] = 0.003 mM in 10 mM phosphate buffer, pH at 7). The peak value of ε at 262 nm, which was consistent with Jin et al. (2006), was selected for spectrophotometric measurement to monitor the decrease in [URD] [2]. The value of ϵ_{254} was estimated to be 8089 ± 334 $M^{-1}cm^{-1}$ through absorbance measurements at 254 nm, which is roughly 10% lower than the value reported by Li et al. (2016) of 8775 $M^{-1}cm^{-1}$ [1].

For the experiments described herein, the initial concentration of uridine in solution ([URD]$_0$) was chosen to be 3 μM, which is roughly one order of magnitude lower than the value of 0.012 mM used by Jin et al. [2]. The reason for selection of this low actinometer concentration was to maintain a low product of $\epsilon \cdot [URD] \cdot l$. In such case, solution absorbance (A_{254}) was maintained below a value of < 0.02, thereby guaranteeing first-order

72 photochemical decay [4]. This was also the value of A_{254} used in experiments involving other
73 chemicals in the capillary reactor, thereby guaranteeing identical UV_{254} exposure among
74 experiments with this system for a given flow rate.
75   A key condition in the use of eq (S1) is a known quantum yield (Φ). Jin et al. reported
76 a quantum yield of 0.020 mol/E, which was the average of three published values [3,5,6]. The
77 quantum yield was estimated independently by the use of a collimated beam UV reactor. Fig.
78 S4 shows the first-order photochemistry of URD under UV_{254nm} irradiation with this
79 collimated beam system.
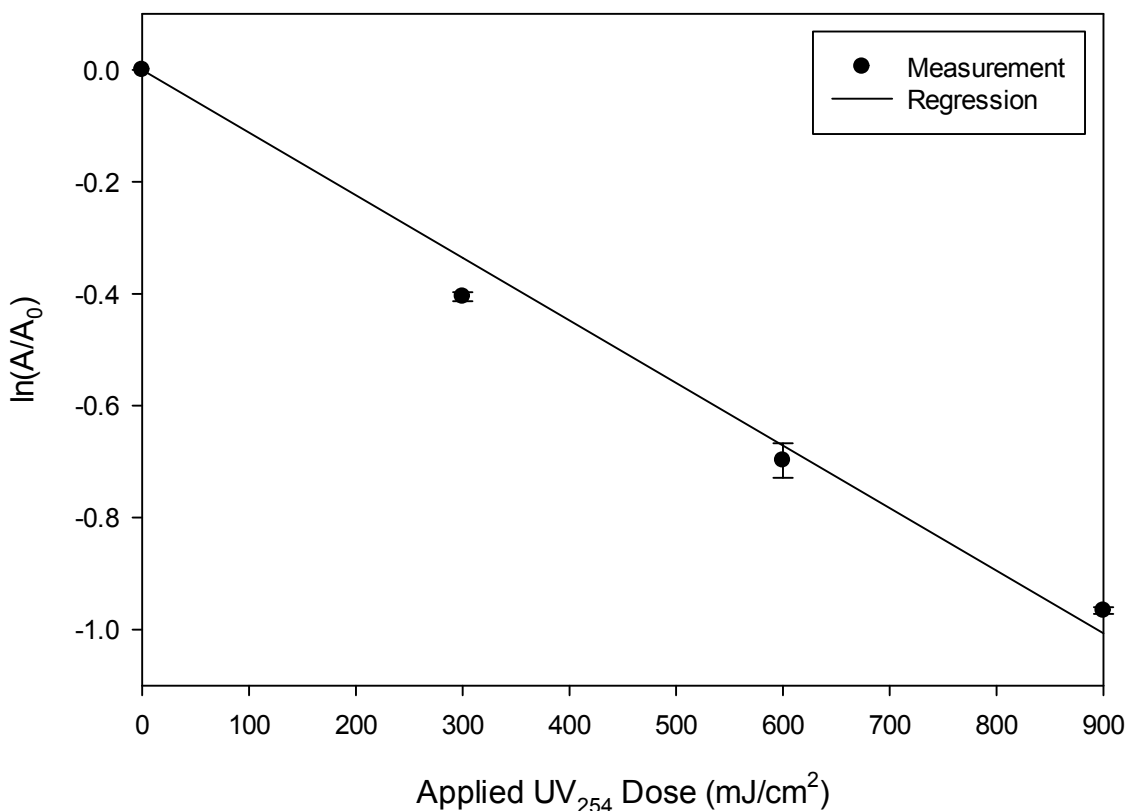
80
81
82   **Figure S4.** First-order photodecay of URD under UV_{254nm} irradiation (pH=7.0, URD]$_0$=3
83   μM, T=25 °C, error bars represent standard deviation of three replicates). Regression was
84   based on an assumed linear relationship between $\ln(A/A_0)$ and applied dose ($R^2 = 0.995$).
85
86   Based on the small optical density ($A(\lambda)<0.02$), the quantum yield of URD was thus
87 estimated as 0.028 ± 0.001 mole/Einstein by eq (S1). Since the rate of photochemical reaction
88 is always governed by the product of $\varepsilon \cdot \Phi$, we assumed that the cause of a higher quantum
89 yield we obtained (as compared with previous studies) to be attributable to the lower molar
90 absorptivity values we observed than were previously reported.
91   Repeatable flow rates were achieved in the experiments by defining pump settings
92 that yielded flow rates of 2.0, 3.0, 4.0, 5.0, 6.0, 7.0, and 8.0 mL/min, and pre-checked by
93 measuring the volume of water passing through the UV lamp in 1 min. It was assumed that
94 the UV_{254} output of the Hg lamp used in the capillary flow reactor was constant, and that
95 because of this the UV_{254} dose delivered to the fluid flowing through the reactor was
96 controlled by flow rate. It was hypothesized that the inverse of flow rate was linearly
97 correlated with the UV dose; this hypothesis was supported by the data presented in Fig. S5.
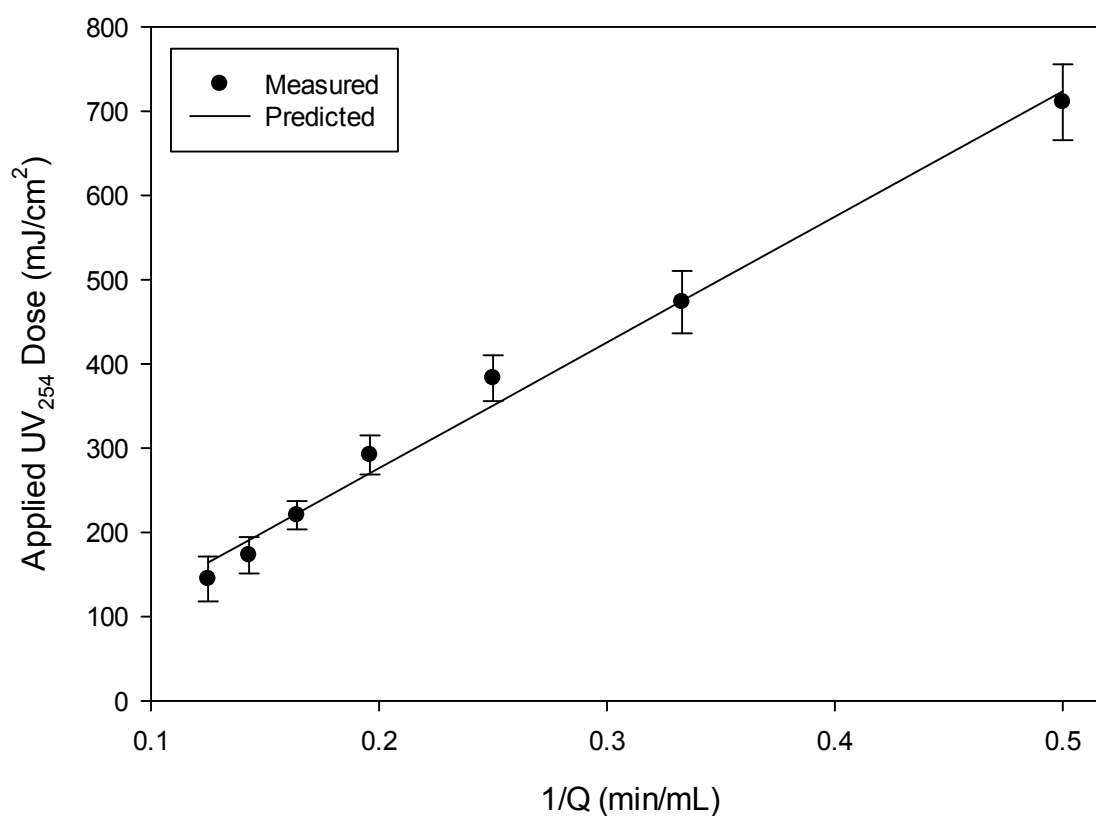
Figure S5. Observed linear relationship between the inverse of flow rate and applied UV_{254} dose delivered by capillary photoreactor, as measured by uridine actinometry (pH=7.0, $[URD]_0$=3 μM, T=25 ℃, error bars represent standard deviation of three replicates; R^2 = 0.990).

105 **Section S3.** Membrane Introduction Mass Spectrometry (MIMS)

106   The MIMS system used in this study was based on an Agilent 6850 bench top GC/MS,
107 comprising an Agilent 5975C quadrupole mass selective detector (MSD) with electron (70
108 eV) ionization. As described in Shang and Blatchley (1999), the membrane cell was
109 constructed around small-diameter silicone tubing, with a liquid flow rate of 0.7 mL/min, and
110 gas (Helium) flow rate at 0.5 mL/min [7]. Volatile reaction products were identified in mass
111 spectrum scan mode (m/z: 49-400 amu), while selected ion monitoring (SIM) mode was
112 applied for quantification of target precursors.

113   In the operation of MIMS connected with a capillary UV system, the stock solution of
114 Cl-DMA was sealed with multiple layers of Parafilm (Flinn Scientific) and injected into the
115 capillary UV reactor operated at a flow rate of 2 mL/min, with the UV lamp off. 10 mins of
116 injection were conducted before collection of treated solution, to avoid any influence caused
117 by adsorption on the tubing system. The UV lamp was then warmed for at least 20 min. Flow
118 rates of 8.0, 5.0, 3.0, and 2.0 mL/min were then established by using the pre-calibrated
119 settings on the pump, and the solution was injected into the capillary UV reactor. After
120 injecting the solution for 5 minutes, the output of the UV reactor was diverted to MIMS, after
121 which 20 mins was allowed to reach a steady-state abundance in the SIM mode on MIMS.

122   The concentration of Cl-DMA in the stock solution should be identical to the
123 concentration of free chlorine added to the solution, $[Cl_2]_0$, 7.04×10^{-5} M. Solutions of $3.52 \times$
124 10^{-5} M and 1.76×10^{-5} M Cl-DMA were prepared by diluting the stock Cl-DMA solution.
125 Standard curves of [Cl-DMA] on MIMS were prepared by injecting different concentrations
126 of Cl-DMA into MIMS and obtaining the steady-state abundance in the SIM mode. The
127 abundance at m/z=78 in the SIM mode was demonstrated to be linearly correlated to the Cl-
128 DMA concentration in solution (Fig. S6). Note that the abundance detected on MIMS for the
129 same solution varied considerably as functions of liquid flow rate or pressure; therefore, each
130 application of MIMS required a new standard curve. Therefore, the curve presented in Fig.
131 S6 is included to illustrate that the abundance was linearly dependent on the concentration.
132 Notice also that in the experimental range of solution concentrations, the abundance was in
133 the range of $10^3 \sim 10^4$.

134
135
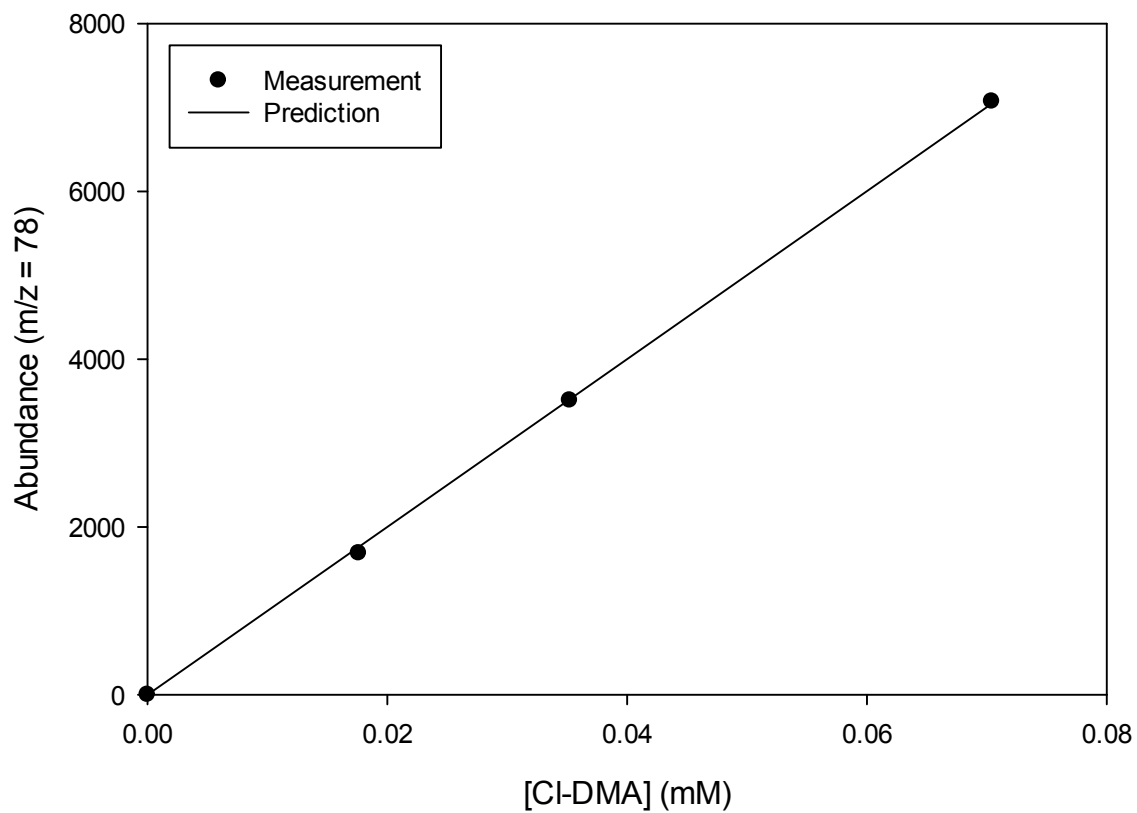
Figure S6. Standard Curve for Cl-DMA on MIMS ($[Cl\text{-}DMA]_0 = 7.04 \times 10^{-5}$ M,
corresponding to 5 mg/L $[Cl_2]$, pH=7.0, T=25 °C; $R^2 = 0.998$).

138

139

140 **Section S4.** DPD and DPD/KI standard curves
141   The DPD and DPD/KI colorimetric methods were well-suited for measuring the free
142 available chlorine (FAC) and +1 valent combined chlorine concentration in aqueous solution.
143 The DPD solution, DPD buffer solution, and experimental procedures were prepared and
144 applied according to *Standard Methods* [8]. Fig. S7 shows one calibration curve of the
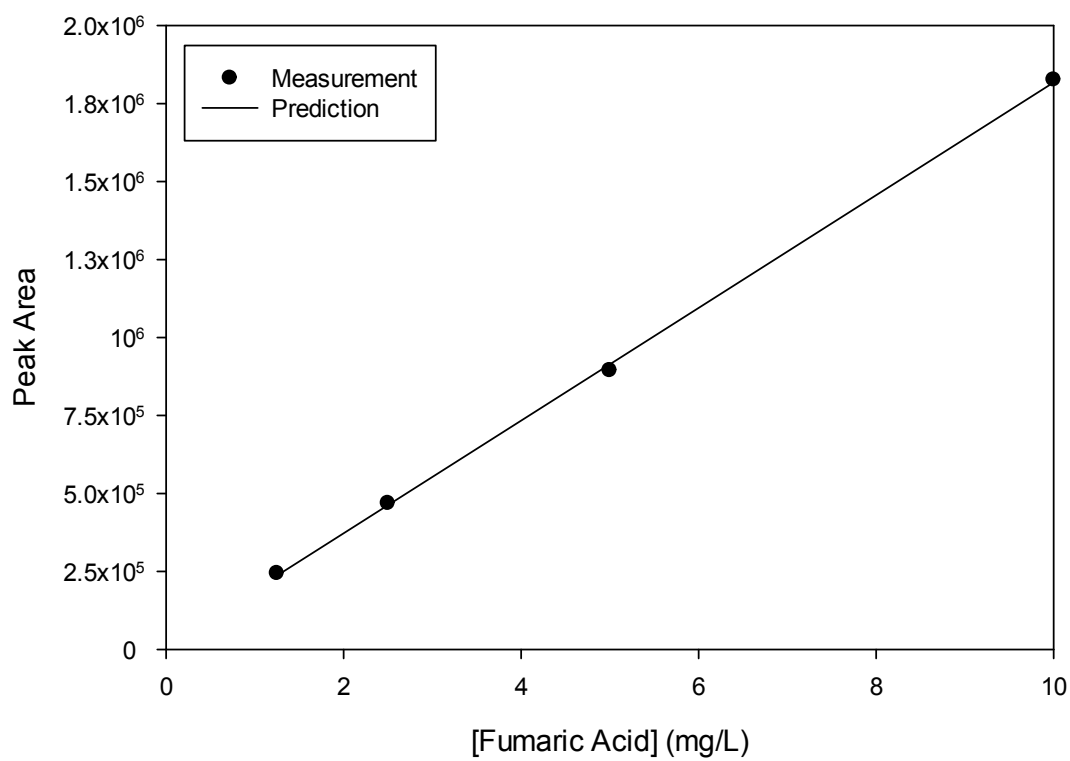145 compound Cl-DMA developed by the DPD/KI method.
146
147
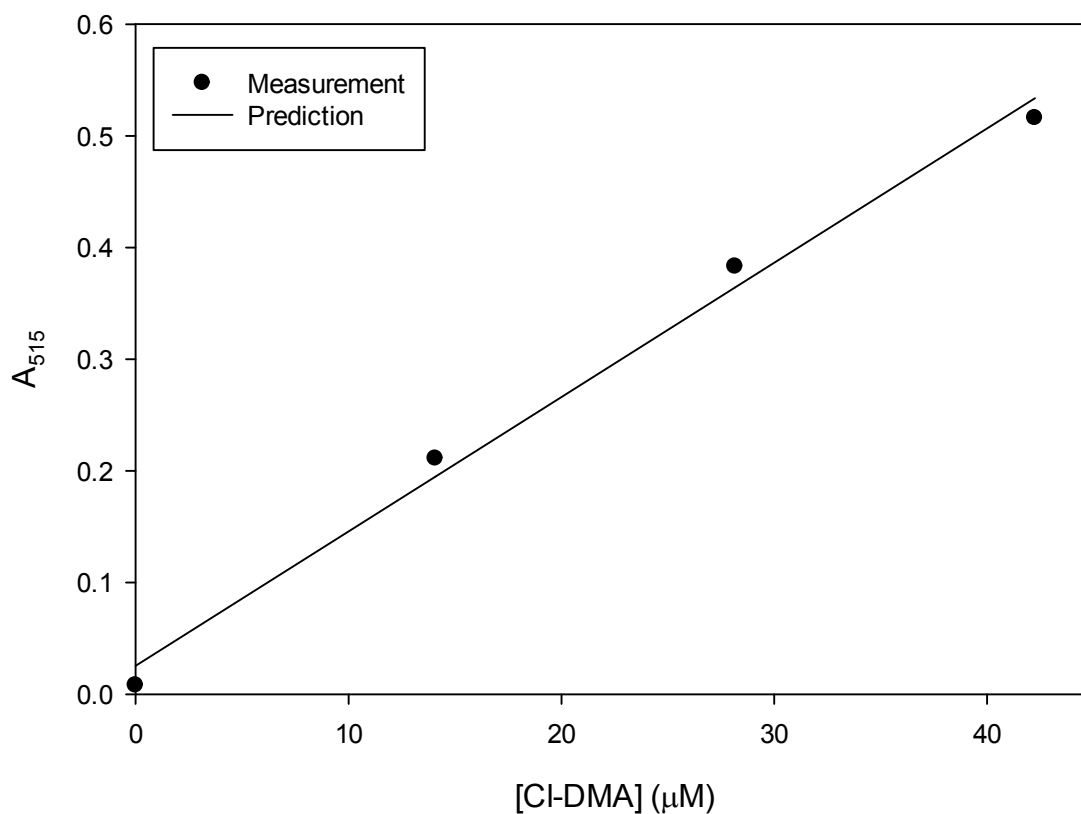
148
149
150   **Figure S7.** Example DPD/KI Colorimetric Method Standard Curve for Cl-DMA.
151
152

153 **Section S5.** Standard Curves of Fumaric Acid and Anatoxin-a on HPLC.   Note that that the
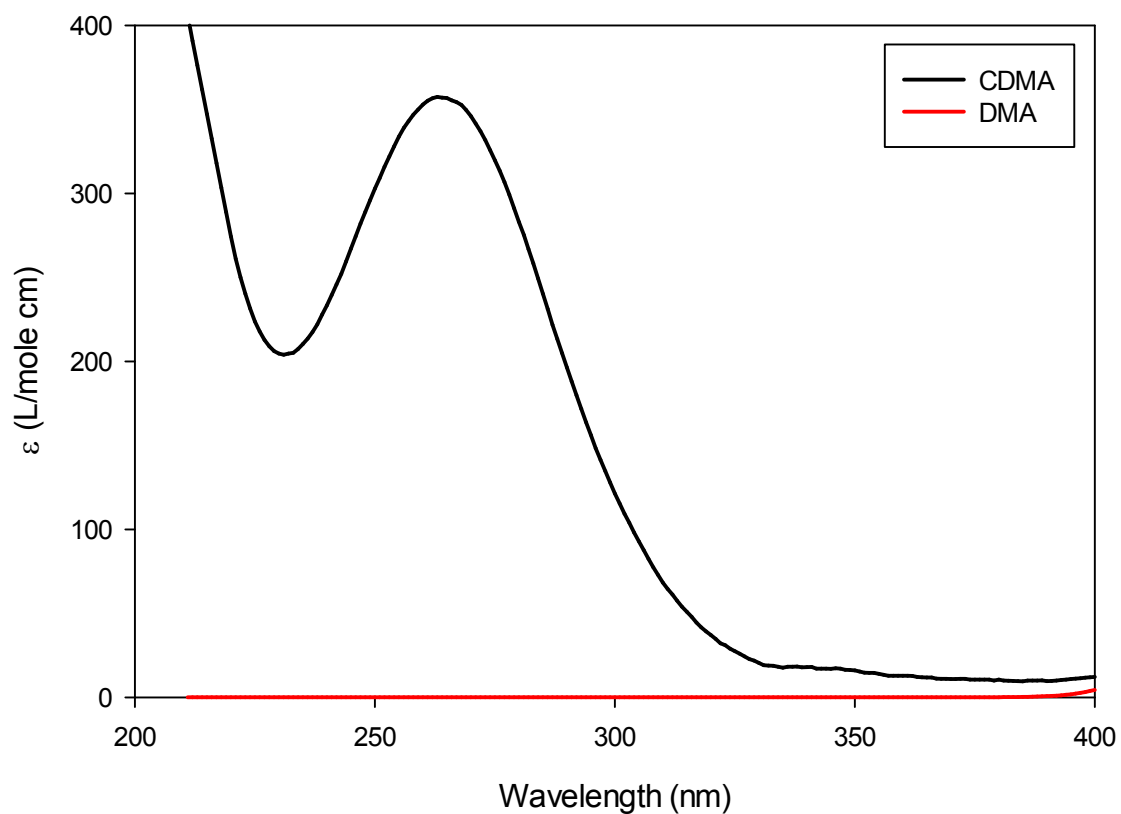154 horizontal axis represents the concentration of ANTX-a (Fumarate) in both figures S9 and
155 S10.

156
157   **Figure S8.** Standard curve for Fumaric Acid in HPLC analysis.
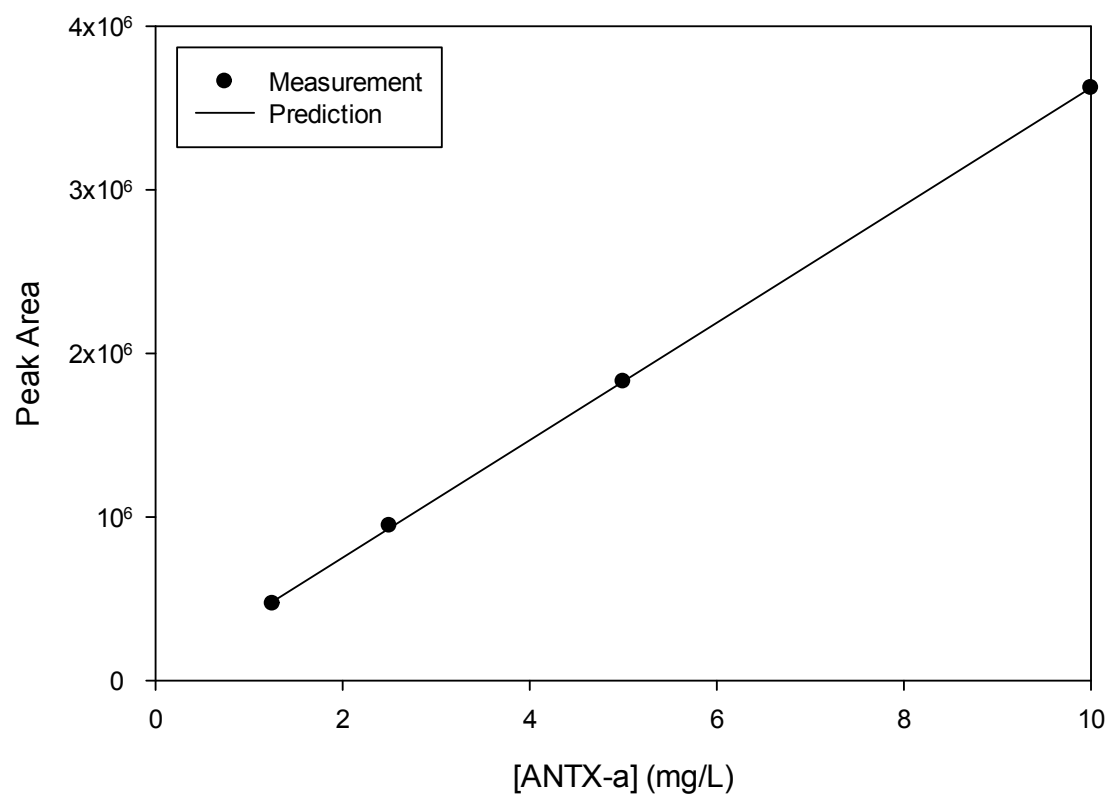
158
159 **Figure S9.** Standard curve for ANTX-a in HPLC analysis.
160

161 **Section S6.** Absorption Spectra of DMA and Cl-DMA

162
163
164 **Figure S10.** Absorption spectra of DMA and Cl-DMA at pH = 7.0 (Cl:N = 1:2 molar
165 ratio).
166
167

168 **Section S7.** Chlorine Demand of ANTX-a
169   In a set of experiments with a Cl:N molar ratio of 5, the peak area readings by HPLC
170 analysis indicated that no detectable ANTX-a existed in the bench reactor within 30 seconds
171 of chlorination. This is conflict with the reported results from Rodriguez et al. [9]. When
172 sodium thiosulfate was added to the solution to quench the chlorine, the peak of ANTX-a
173 returned to its original form (Fig. S11). A subsequent set of experiments indicated that with a
174 Cl:N molar ratio of 1.0, 90% of free chlorine was depleted within 1 min, and over 99% of
175 free chlorine was depleted within 10 min; however, when a KI crystal was added to the
176 solution, the solution instantly became pink and a stable reading at 515 nm was obtained. As
177 described in Section S4, this is an indication that +1 valent chlorine existed in the solution in
178 the form of combined chlorine. These observations indicated that the behavior of ANTX-a in
179 chlorination is quite similar to DMA, in that electrophilic substitution occurred at the
180 secondary amine structure, resulting in formation of an N-Cl bond. Therefore, it became
181 apparent that the chlorination of ANTX-a is a rapid process, but such effect could be masked
182 by the addition of thiosulfate, as used by Rodriguez et al.[9].
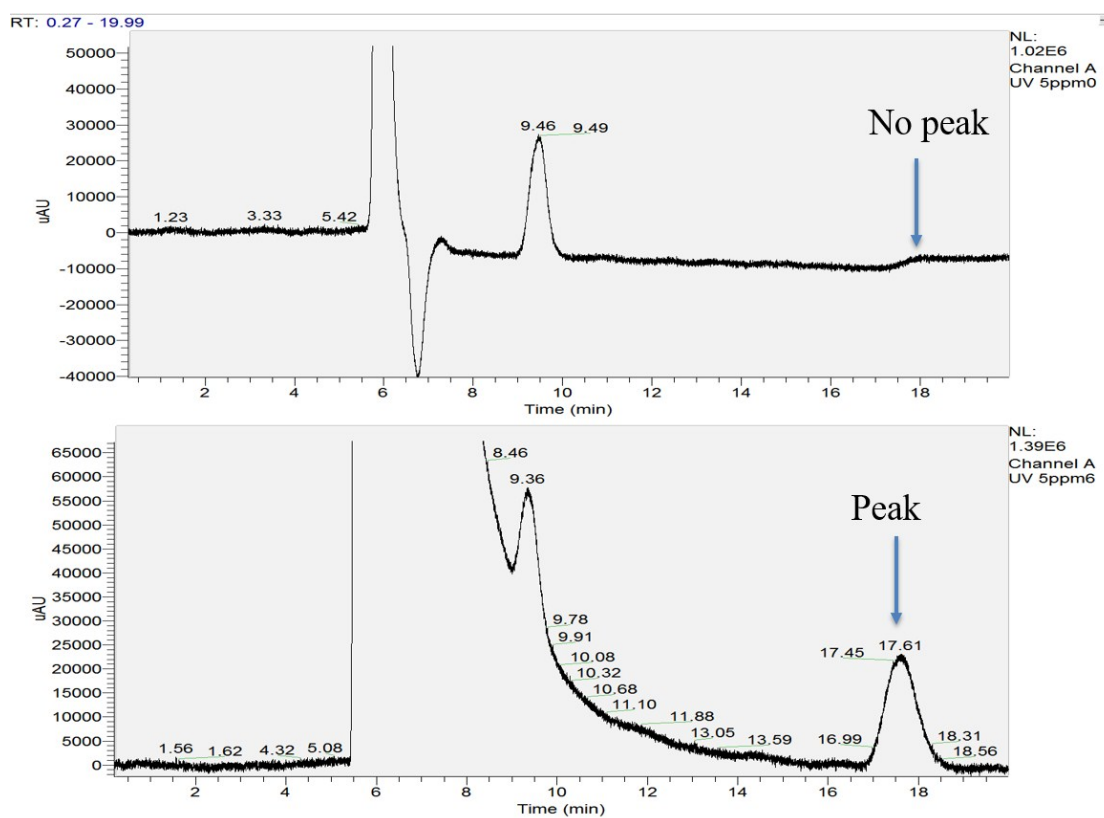
184 **Figure S11.** Recovery of the ANTX-a HPLC peak of by addition of sodium thiosulfate.
185

186   To further support this, we analyzed for the formation of Cl-ANTX-a by the DPD/KI
187 colorimetric method. In a set of experiments with different concentrations of ANTX-a and
188 free chlorine, but constant Cl:N ratio of 1.4, DPD/KI analysis was conducted after mixing
189 ANTX-a and free chlorine for 10 min. At this point, no free chlorine was detected in either of
190 these solutions. However, after adding KI crystals, the pink color appeared instantly and a
191 stable reading at 515 nm was obtained for each solution. Therefore, in these solutions, we
192 regarded that the concentrations of Cl-ANTX-a were identical to that of the original ANTX-a,
193 0, 0.8, 1.7, 3.5 μM.
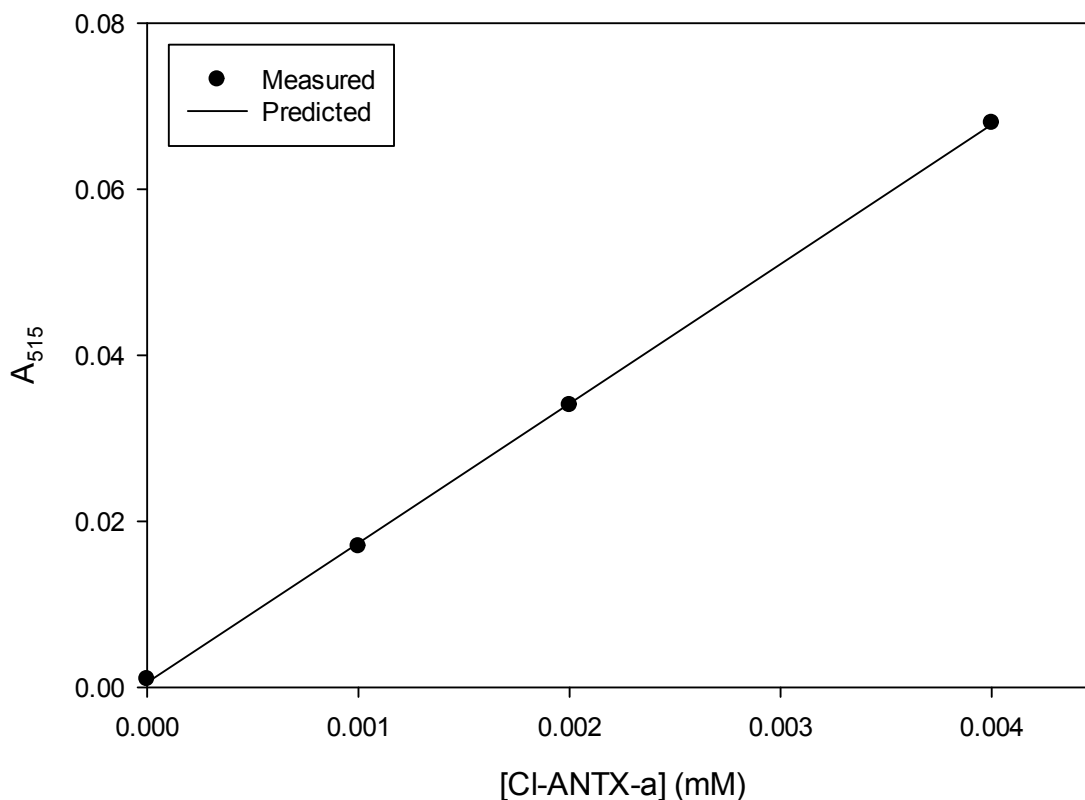
194

195

196   **Figure S12.** Standard Curve for Cl-ANTX-a by DPD/KI Colorimetric Method

197

198   Several bench experiments involving 11 mL of working solution with a Cl:N molar
199 ratio of 1~2 were prepared. The HPLC was used to observe the disappearance of ANTX-a,
200 while DPD and DPD/KI colorimetric methods were used to detect residual free chlorine and
201 combined chlorine. In a typical experiment, the initial concentration of ANTX-a (Fumarate)
202 was 5 mg/L (0.0178 mM), pH was adjusted at 7 by NaOH or HCl in the presence of 10 mM
203 phosphate buffer, at room temperature (~22°C). 1 mL of the working solution was rapidly
204 transferred into an HPLC vial and analyzed every 20 minutes. The rest of the solution was
205 kept in the dark in a brown container. When the peak area of ANTX-a became stable in two
206 successive HPLC analyses, and when the peak area of ANTX-a became unreadable in HPLC
207 chromatogram in two successive analyses, a DPD measurement was applied on the rest of the
208 solution to check the existence of residual free chlorine.

209   Since it had been shown that there was no free chlorine in the 1:1 scenario, and about
210 25% of $[ANTX-a]_0$ still remained in the solution (Fig. S13), it was assumed that the
211 approximate free chlorine demand of ANTX-a was 1.3~1.4 times $[ANTX-a]_0$, on a molar
212 basis.
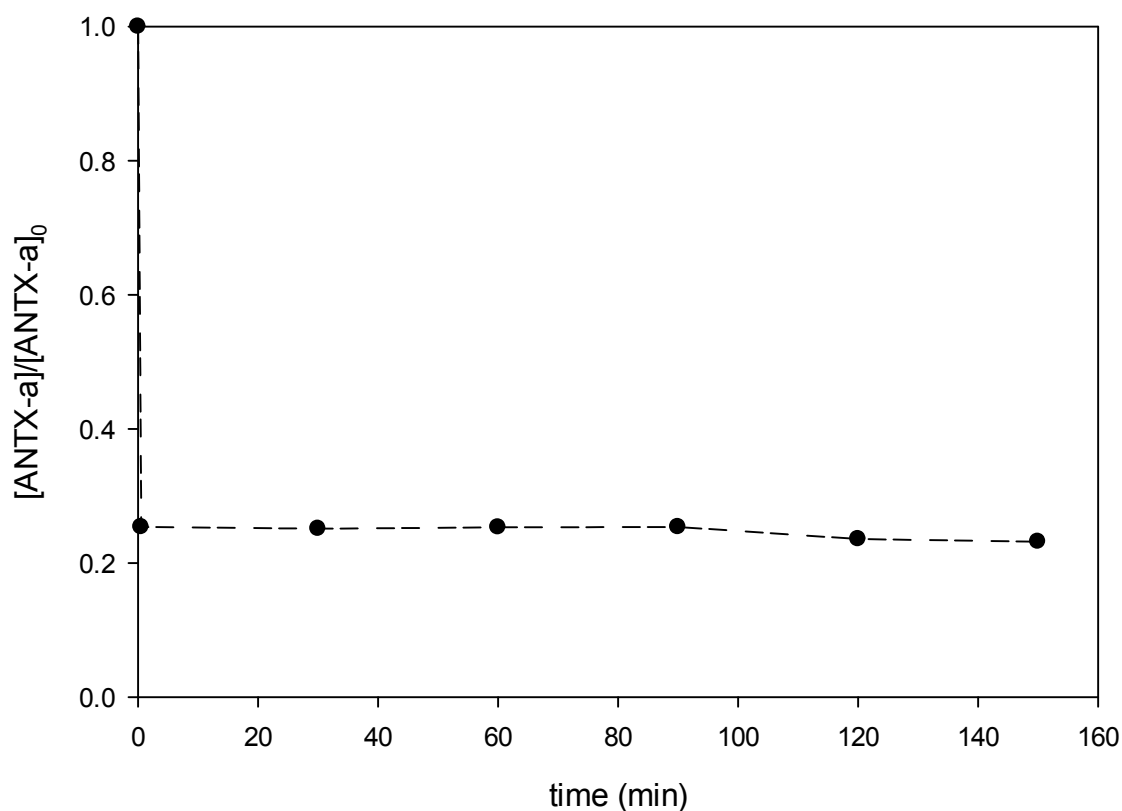
215 **Figure S13.** ANTX-a loss in Cl:N= 1:1 scenario.
216

217   To specify the chlorine demand of ANTX-a, two more sets of experiments involving
218 chlorination of ANTX-a were conducted. 1 mL of solution was transferred quickly into an
219 HPLC vial and analyzed every 20 min. In the scenario of Cl:N=1.3:1, successive analyses at
220 40 and 60 min showed essentially identical peak areas on the HPLC, and the analysis was
221 stopped. The DPD colorimetric method results indicated that at both times, the solution after
222 adding 0.5 mL DPD was transparent, and the A_{515} value was zero. In the scenario of
223 Cl:N=1.4:1, two successive analyses at 40 and 60 min showed no detectable peak by HPLC
224 and the analysis was stopped. DPD colorimetric method results also indicated that at these
225 times, no free chlorine was present. Therefore, the free chlorine demand was assumed to be
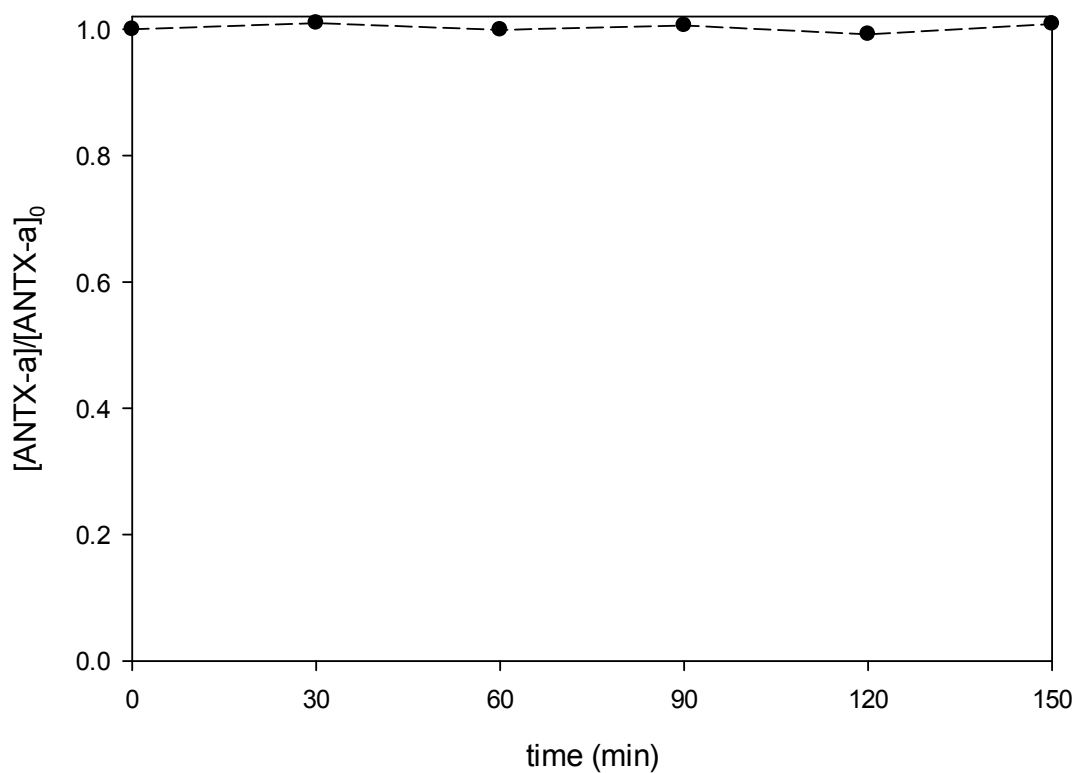226 roughly 1.4:1 on a molar basis.

227

228 **Section S8.** Control group experiments.
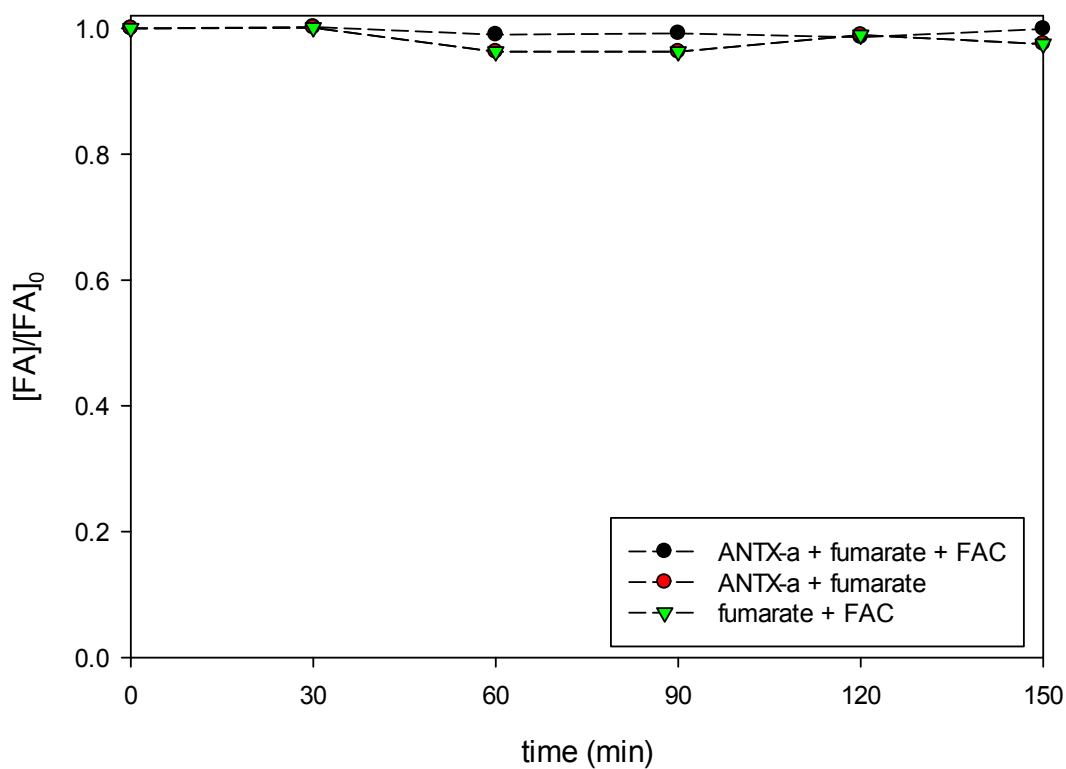
229
230 **Figure S14.** Effect of chlorine on fumaric acid (FA). ([ANTX-a-Fumarate] = 5 mg/L, pH=7).


231
232 **Figure S15.** Stability of ANTX-a during the experimental period. (T=25 °C, [ANTX-a-
233 fumarate] = 5 mg/L, pH=7).

234 **Section S9.** Direct UV Photolysis of ANTX-a
235   For each experiment with ANTX-a, a solution containing 6 mL of ANTX-a (fumarate) at
236 5 mg/L in 20 mM phosphate buffer was prepared and contained in a plastic Petri dish with a
237 diameter of 4.7 cm. 250 μL samples were collected and placed into an HPLC vial at a time
238 interval of 15 min under the collimated beam UV_{254} device. Changes in solution volume and
239 the volume of the stirring bar were considered in the calculation of the dose applied to the
240 solution. The pH was adjusted with NaOH and HCl. Solution pH was measured before and
241 after each experiment. It was anticipated that absorption spectra would demonstrate pH-
242 dependence for ANTX-a because of the acid/base behavior of their functional groups. The
243 absorption spectra of ANTX-a measured for 200 nm $\leq \lambda \leq$ 400 nm are shown in Fig. S16
244 below.
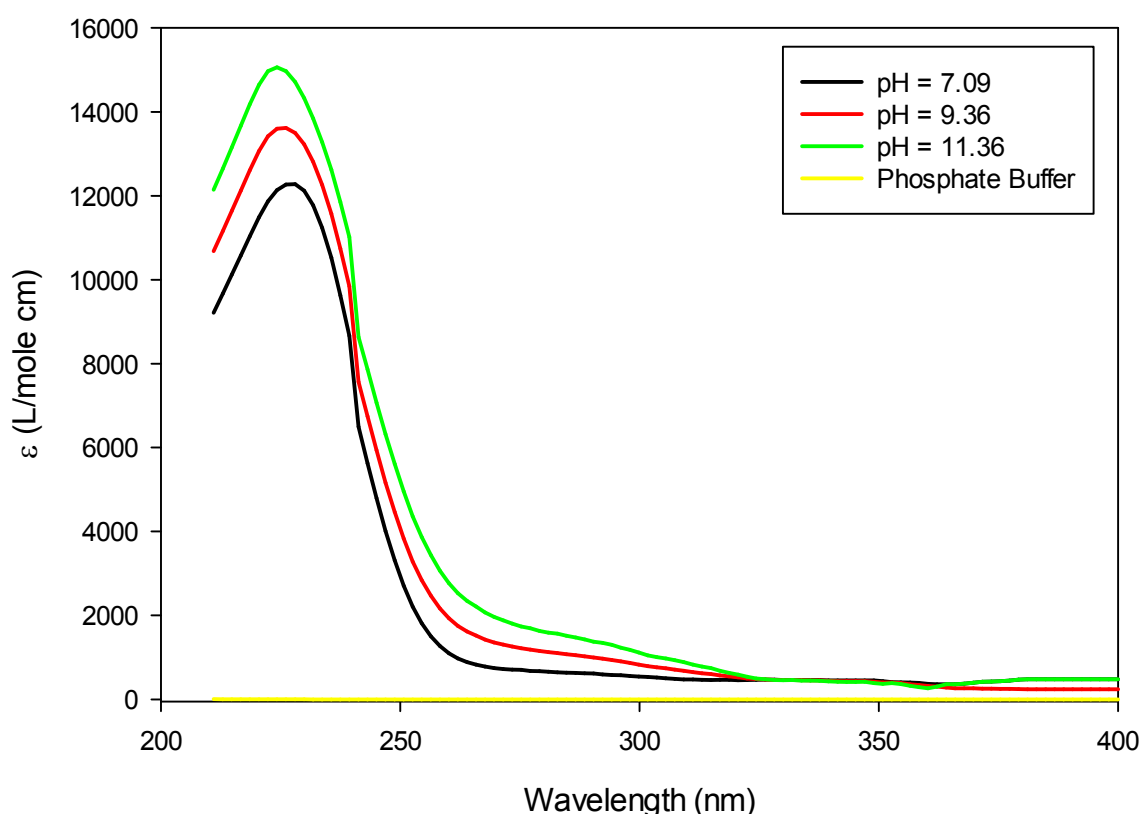
245
246
247 **Figure S16.** UV Absorption Spectra of ANTX-a at several pH values near to its pK_a (9.36).
248 Phosphate buffer do not absorb comparable UV radiation to ANTX-a at all three pHs. (T=25
249 ℃, 10 mM phosphate buffer, [ANTX-a-Fumarate] = 1 mg/L, Subtracting Effect of Fumaric
250   Acid).
251
252
253

254 **Section S10.** UV Photodegradation of Cl-ANTX-a
255   Considering the possible loss of free chlorine under a collimated beam UV reactor in
256 a fume hood, a capillary UV reactor was chosen as the device for UV exposure in treating Cl-
257 ANTX-a. Encouraged by the similar behaviors of ANTX-a and DMA in chlorination, several
258 stock solutions of a 100-mL volume containing known Cl:N molar ratios were freshly
259 prepared for Cl-ANTX-a with a Cl:N molar ratio of 1.4, as discussed in Section 3.1.2. A
260 freshly prepared Cl-ANTX-a solution ($[ANTX-a]_0$=3.55 * 10^{-6} M, 10 mM phosphate buffer,
261 pH=7.0) was sealed with multiple layers of Parafilm (Flinn Scientific) and injected into the
262 capillary UV reactor connected at a flow rate of 2 mL/min. Notice that for solutions of Cl-
263 ANTX-a and the actinometer, the absorbance was controlled to be close to 0, so that their
264 degradation could be approximated as first-order; this also ensured that the fluence rate field
265 within the reactor was essentially identical for experiments with both compounds. This
266 allowed direct comparison of the data from experiments with Cl-ANTX-a and the
267 actinometer. 10 mins of injection were conducted before collection of treated solution, to
268 avoid any influence caused by adsorption on the tubing system. The UV lamp was warmed
269 for at least 20 min. Flow rates of 8.0, 5.0, 3.0, and 2.0 mL/min were then established by using
270 the pre-calibrated settings on the pump, and the solution was injected into the capillary UV
271 reactor. After each sample collection, 1 mL was transferred into an HPLC vial (for
272 determination of residual fumaric acid), and the rest of the solution was diluted by a factor of
273 two, then subjected to the DPD/KI colorimetric assay to determine the residual free and
274 combined chlorine. In this method, the readings by the DPD/KI method for combined +1
275 valent chlorine were used as a surrogate measurement for the concentration of Cl-ANTX-a. A
276 standard curve obtained through this method is shown in Fig. S12.
277   Cl-DMA solutions ($[Cl-DMA]_0$=7.04 × 10^{-5} M, 10 mM phosphate buffer, pH=7.0)
278 were freshly prepared for each experiment and injected into the capillary UV system
279 connected directly to MIMS. As with the experiments described above for Cl-ANTX-a, the
280 absorbance of Cl-DMA and actinometer solutions was controlled to be close to 0, so that their
281 degradation could be approximated as first-order and the results of two compounds could be
282 compared directly. For each known UV dose applied to the Cl-DMA solution, MIMS was
283 used to quantify the concentration of [Cl-DMA]. A standard curve of [Cl-DMA] for the
284 MIMS system is shown in Fig. S6. A control experiment was conducted with the UV lamp
285 off; no change in [Cl-DMA] was observed under this condition.
286
287
288
289

290
291

292 **Section S11.** Stability of Cl-ANTX-a
293　　　　Since a DPD/KI test from Heeb et al. indicated only a 7% loss in Cl-DMA over a
294 period of 24 h when the stock solution was stored in the dark, self-decay of Cl-DMA was not
295 considered over the experimental period.[10]
296　　　　Several experiments were carried out and tested by HPLC to verify the stability of
297 chlorinated ANTX-a. In these experiments, thiosulfate and/or free chlorine were added (see
298 scenario descriptions in caption for Fig. S17). As shown in Fig. S17, comparison of scenarios
299 A and B illustrated the effect of sodium thiosulfate on ANTX-a; no effect was observed. Also,
300 comparison of scenarios B and C indicated that chlorination occurred on a position that could
301 be reversed by thiosulfate. As this behavior of the chlorination of ANTX-a was similar to that
302 of DMA, and as the behavior was quite consistent with N-chlorination, it was assumed that
303 the primary location for chlorine substitution of ANTX-a was on the secondary amine, as
304 with DMA, and the main product was Cl-ANTX-a.
305
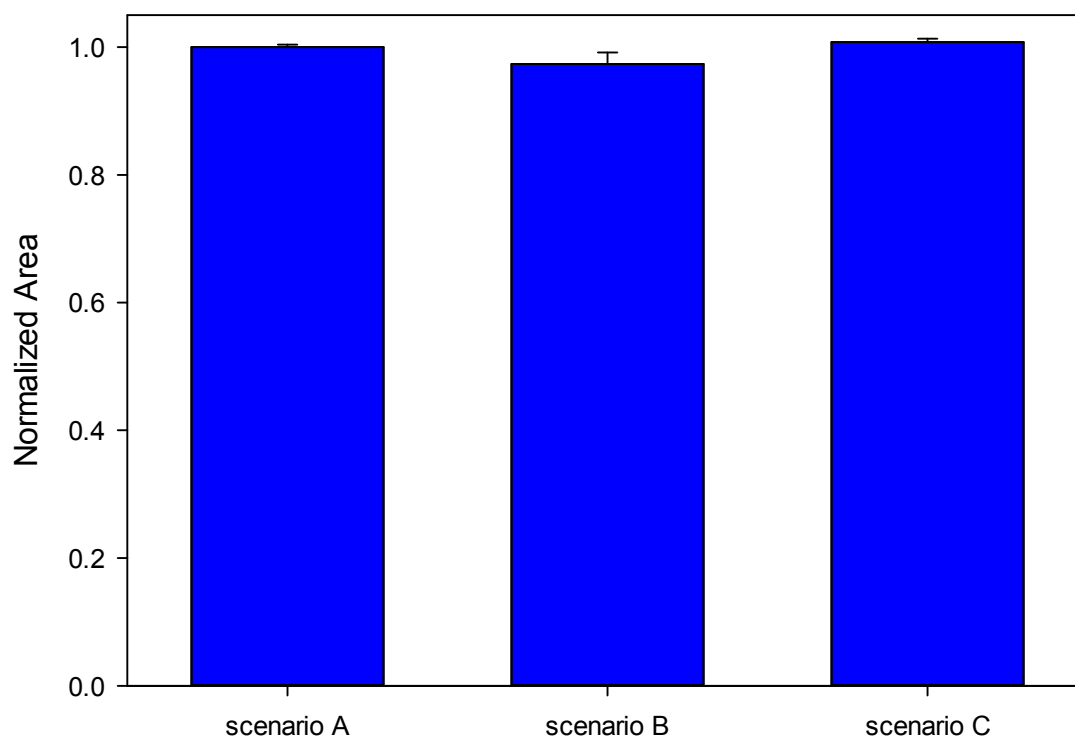
307 **Figure S17.** Consistency of　HPLC analysis for Cl-ANTX-a with sodium thiosulfate.
308　 Scenario A: no free chlorine, no thiosulfate; Scenario B: only thiosulfate; Scenario C: free
309　chlorine and thiosulfate; (Normalized to Scenario A. [Cl-ANTX-a] = 3.6 μM, corresponding
310 to 1 mg/L of ANTX-a-Fumarate, pH at 7.00, T=25 °C, error bars represent standard deviation
311　　　　　　　　　　　　　　　　of two analyses).

312　　　The DPD/KI colorimetric assays illustrated that chlorination of ANTX-a reached
313 completion after 60 min. Time-course samples were collected and analyzed by HPLC with
314 sodium thiosulfate and DPD/KI colorimetric method and it was expected that over the
315 experimental period Cl-ANTX-a would be stable. As shown in Fig. S19, the consistent
316 readings by HPLC and the absorption at 515 nm in the DPD/KI colorimetric method

317 throughout the experimental period indicated that Cl-ANTX-a has little ability to self-degrade,
318 at least on the timescale of these experiments.

319
320

321
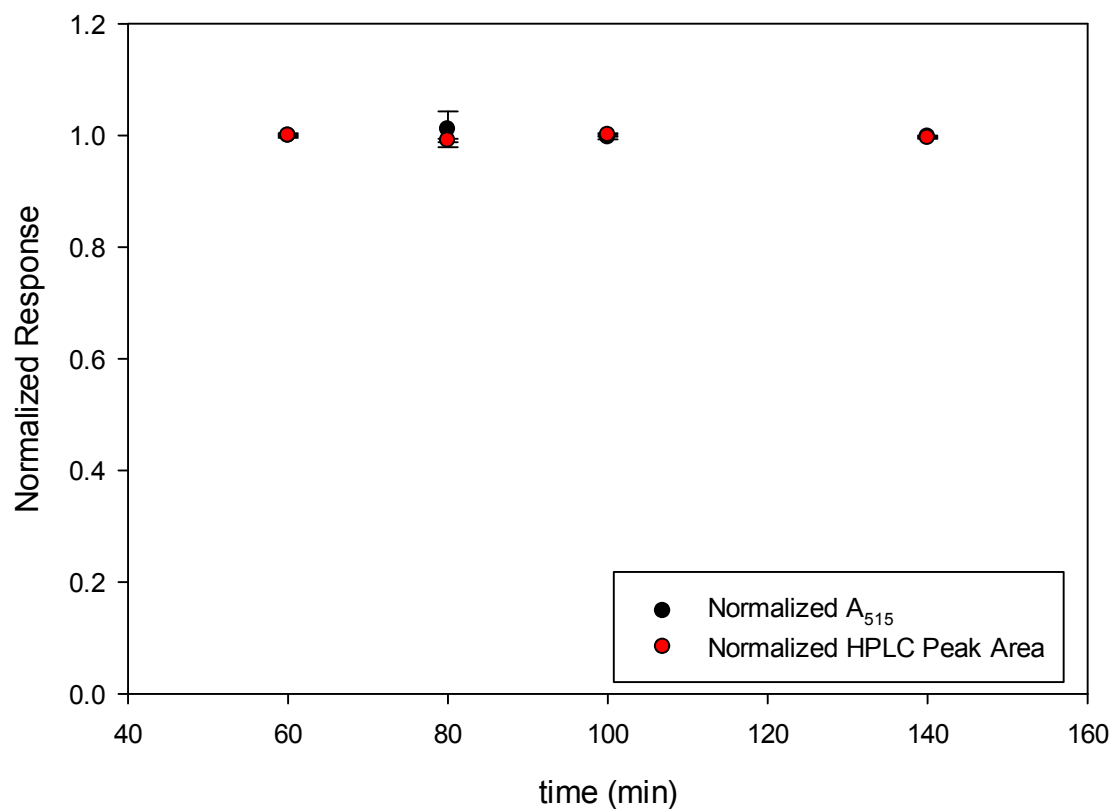
Figure S18. Stability of Cl-ANTX-a during an 80-min experimental period.
(Normalized to readings at t = 60 min. [Cl-ANTX-a] = 3.6 $\times$ 10^{-6} M, corresponding to 1
mg/L of ANTX-a-Fumarate, pH at 7.00, T=25 °C, error bars represent standard deviation of
two analyses).

326

327 **Section S12.** Absorption Spectra of ANTX-a and N-Chloro-ANTX-a (pH at 7)
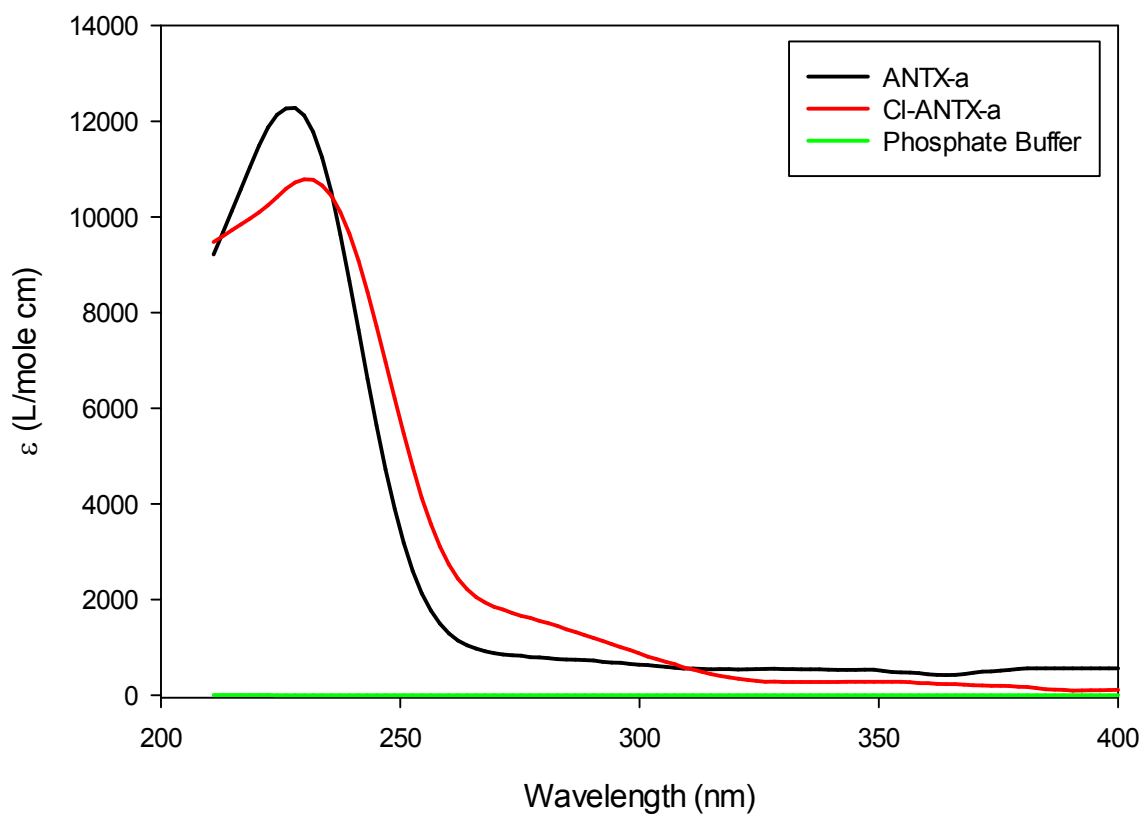
328
329
330 **Figure S19.** Absorption Spectra of ANTX-a and Cl-ANTX-a (pH=7.00, 10 mM phosphate
331   buffer, T=25 ℃, $[C]_0$=3.6 × 10^{-6} M).

References

1   M. Li, Z. Qiang, P. Hou, J. R. Bolton, J. Qu, P. Li and C. Wang, VUV/UV/Chlorine as an Enhanced Advanced Oxidation Process for Organic Pollutant Removal from Water: Assessment with a Novel Mini-Fluidic VUV/UV Photoreaction System (MVPS), *Environ. Sci. Technol.*, 2016, **50**, 5849–5856.

2   S. Jin, A. a Mofidi, M. Asce and K. G. Linden, Polychromatic UV Fluence Measurement Using Chemical Actinometry, Biosimetry, and Mathematical Techniques, *J. Environ. Eng.*, 2006, **132**, 831–842.

3   P. A. Swenson and R. B. Setlow, Kinetics of Dimer Formation and Photohydration in Ultraviolet-Irradiated Polyuridylic Acid, *Photochem. Photobiol.*, 1963, **2**, 419–434.

4   J. R. Bolton, I. Mayor-Smith and K. G. Linden, Rethinking the Concepts of Fluence (UV Dose) and Fluence Rate: The Importance of Photon-based Units - A Systemic Review, *Photochem. Photobiol.*, 2015, **91**, 1252–1262.

5   R. L. . Sinsheimer, The Photochemistry of Uridylic Acid, 1954, **1**, 505–513.

6   B. K. G. Linden and J. L. Darby, Estimating Effective Germicidal Dose from Medium Pressure UV Lamps, 1997, **123**, 1142–1149.

7   C. Shang and E. R. Blatchley, Differentiation and quantification of free chlorine and inorganic chloramines in aqueous solution by MIMS, *Environ. Sci. Technol.*, 1999, **33**, 2218–2223.

8   S. Methods, *Standard methods for the examination of water and wastewater*, *Standard methods for the examination of water and wastewater*, 1998.

9   E. Rodríguez, A. Sordo, J. S. Metcalf and J. L. Acero, Kinetics of the oxidation of cylindrospermopsin and anatoxin-a with chlorine, monochloramine and permanganate, *Water Res.*, 2007, **41**, 2048–2056.

10 M. B. Heeb, I. Kristiana, D. Trogolo, J. S. Arey and U. von Gunten, Formation and reactivity of inorganic and organic chloramines and bromamines during oxidative water treatment, *Water Res.*, 2017, **110**, 91–101.